# Midinfrared-light-induced ferroelectricity in oxide paraelectrics via nonlinear phononics

Alaska Subedi

*Centre de Physique Theorique, Ecole Polytechnique, CNRS, Université Paris-Saclay, F-91128 Palaiseau, France*
*and Collège de France, 11 place Marcelin Berthelot, 75005 Paris, France*

I show that a nonequilibrium paraelectric to ferroelectric transition can be transiently induced using midinfrared pulses. This relies on a quartic $l Q_{l_z}^2 Q_{h_x}^2$ coupling between the lowest ($Q_{l_z}$) and highest ($Q_{h_x}$) frequency infrared-active phonon modes of a paraelectric material. Density functional calculations show that the coupling constant $l$ is negative, which causes a softening of the $Q_{l_z}$ mode when the $Q_{h_x}$ mode is externally pumped. A rectification along the $Q_{l_z}$ coordinate that stabilizes the nonequilibrium ferroelectric state occurs only above a critical threshold for the electric field of the pump pulse, demonstrating that this is a nonperturbative phenomenon. A first-principles calculation of the coupling between light and the $Q_{h_x}$ mode shows that ferroelectricity can be induced in the representative case of strained $KTaO_3$ by a midinfrared pulse with a peak electric field of $17\,\mathrm{MV\,cm^{-1}}$ and duration of 2 ps. Furthermore, other odd-order nonlinear couplings make it possible to arbitrarily switch off the light-induced ferroelectric state, making this technique feasible for all-optic devices.

## I. INTRODUCTION

Living organisms have used light to observe the properties of materials since the evolutionary development of complex eyes. However, ultrafast light-control of materials properties has only become feasible after the construction of high-powered lasers in the previous century, and this field has flourished because light-induced processes have the potential to lead to new devices and physical phenomena. Many examples of light-induced phase transitions using near-visible sources have been observed, including discontinuous volume changes in polymer gels [1], quasi-ionic-to-quasineutral transition in organic molecular compounds [2], low-spin to high-spin transition in metal organic frameworks [3], insulator-to-metal transition in perovskite manganites [4], and, remarkably, a transition to a hidden metastable state in $1T$-$TaS_2$ [5]. All of these examples involve transition to higher-temperature or metastable phases, and the quest to stabilize a phase with less symmetry or more order using light remains elusive.

More recently, intense midinfrared pulses have been used to directly control the dynamical degrees of freedom of the crystal lattice. Such mode-selective vibrational excitations have been used to induce insulator-to-metal transitions [6,7] and melting of orbital [8] and magnetic [9,10] orders. Midinfrared excitations have so far not caused transitions to more-ordered phases, although light-induced superconductivity has been claimed in several cuprate compounds and $K_3C_{60}$ [11–14]. However, these claims rely on interpreting the two-dimensional response function $\Sigma(\omega,\tau)$ measured in the pump-probe experiments as the optical conductivity $\sigma(\omega)$ that is measured in time-domain spectroscopy. It is unclear whether such an interpretation is justified, especially at low frequencies, when the light-induced state is short-lived, as is the case in these experiments [15,16]. In any case, a light-induced transition to a lower-symmetry phase is not observed in any of these experiments. Nonetheless, midinfrared excitation should be an effective tool to drive materials to broken-symmetry phases because selective and coherent excitation of the low-energy structural degrees of freedom should cause minimal dissipation as heat.

The mechanism for mode-selective light-control of materials was proposed by Först *et al.* [17,18]. This involves exciting

an infrared-active phonon mode $Q_{IR}$ of a material using an intense light pulse which then causes the lattice to displace along a fully symmetric $A_g$ Raman mode coordinate $Q_R$ due to a nonlinear coupling $Q_R Q_{IR}^2$ between the two modes. A quantitative microscopic theory of this phenomenon was developed in Ref. [19], and calculations based on this theory in combination with a time-resolved x-ray diffraction experiment was used to resolve the midinfrared-light-induced changes in the structure of $YBa_2Cu_3O_{6.5}$ [20]. In addition to the historically discussed cubic order $Q_R Q_{IR_1} Q_{IR_2}$ coupling [21,22], Subedi *et al.* have shown that a sizable quartic order $Q_R^2 Q_{IR}^2$ coupling can occur and studied the dynamics due to such a coupling [19]. They found that such a quartic coupling exhibits various distinct regimes of dynamics, including transient mode softening and dynamic stabilization in a rectified state. In contrast to the case of the cubic coupling, the displacement along the $Q_R$ coordinate occurs only above a critical pump amplitude threshold for the quartic $Q_R^2 Q_{IR}^2$ coupling. A more recent work has reproduced several aspects of the dynamics of this coupling [23]. Unlike the cubic $Q_R Q_{IR_1} Q_{IR_2}$ coupling [24], the $Q_R^2 Q_{IR}^2$ coupling can cause a rectification along a symmetry breaking mode [19], but such a light-induced symmetry breaking of a crystal structure has so far not been observed.

It has recently been predicted that ferroelectric polarization can be switched using midinfrared pulses [25]. In this paper, I extend that work to the paraelectric phase and show that ferroelectricity can also be transiently induced in transition metal oxide paraelectrics. This relies on a quartic $l Q_{l_z}^2 Q_{h_x}^2$ coupling and is a nonperturbative effect that occurs only above a critical pump amplitude. Here, $Q_{h_x}$ is a high-frequency infrared-active phonon mode that should be externally pumped and $Q_{l_z}$ is the lowest frequency infrared-active mode that is transverse to the pumped mode. I find that the sign of the coupling constant $l$ is negative in several transition metal oxides, which causes the $Q_{l_z}$ mode to soften as the $Q_{h_x}$ mode is externally pumped. But other quartic order couplings $t_1 Q_{l_x}^3 Q_{h_x}$, $t_2 Q_{l_x}^2 Q_{h_x}^2$, and $t_3 Q_{l_x} Q_{h_x}^3$ between $Q_{h_x}$ and the lowest frequency mode $Q_{l_x}$ that is longitudinal to the pumped mode are larger in magnitude. In the cubic materials, the couplings

between $Q_{1_x}$ and $Q_{h_x}$ modes are such that the $Q_{1_z}$ mode may not develop a light-induced dynamical instability. However, I find that the couplings in the longitudinal direction can be effectively reduced by applying strain so that a light-induced ferroelectric state is stabilized by rectification along the $Q_{1_z}$ coordinate.

I illustrate this theory for the representative case of $KTaO_3$ to show that light-induced ferroelectricity can be generated in the strained version of this material when a pump pulse with an electric field of $\sim 17 \ MV \ cm^{-1}$ and pulse duration of 2 ps is used. Interestingly, this value is noticeably smaller than what is expected for the critical pump amplitude due to a $Q_{1_z}^2 Q_{h_x}^2$ coupling [19]. I find that this reduction is due to the presence of substantial sixth-order $Q_{1_z}^4 Q_{h_x}^2$ and $Q_{1_z}^2 Q_{h_x}^4$ couplings. Furthermore, I show that the light-induced rectification can be arbitrarily suppressed by pumping the highest frequency infrared-active mode $Q_{h_x}$ that is longitudinal to $Q_{1_x}$ with another weak pulse. Such a control is necessary for applications in devices. In addition to $KTaO_3$, I find similar nonlinear couplings in $SrTiO_3$ and $LaAlO_3$, and this technique could be generally applied to many transition metal oxide paralectrics.

## II. APPROACH

### A. Computational details

The phonon frequencies and eigenvectors, nonlinear couplings between different normal mode coordinates, and the coupling between light and pumped infrared mode were all obtained from first principles using density functional calculations as implemented in the VASP software package [26]. I used the projector augmented wave pseudopotentials provided with the package with the electronic configurations $3s^2 3p^6 4s^1$ (K), $5p^6 6s^2 5d^3$ (Ta), and $2s^2 2p^4$ (O, normal cut-off) [27,28]. A plane-wave cutoff of 550 eV for basis-set expansion, an $8 \times 8 \times 8$ $k$-point grid for Brillouin zone sampling, and the PBEsol version of the generalized gradient approximation was used [29].

The calculations were done using the relaxed lattice parameters for the cubic structure. For the strained structure, the $c$ lattice parameter that minimized the total energy for the given strain was used. A very small energy convergence criteria of $10^{-8}$ eV was used in the calculations to ensure high numerical accuracy. After relaxing the lattice parameters, I calculated the phonon frequencies and eigenvectors using the frozen phonon method as implemented in the PHONOPY software package [30,31]. After the normal mode coordinates were identified, total energy calculations were performed as a function of the $Q_{1_z}$, $Q_{1_x}$, and $Q_{h_x}$ coordinates for values ranging between $-3$ and 3 $\text{Å}\sqrt{\text{amu}}$ with a step of 0.1 $\text{Å}\sqrt{\text{amu}}$ to obtain the energy surfaces $V(Q_{1_z}, Q_{1_x}, Q_{h_x})$. These were then fitted to polynomials given in Eq. (A1) to obtain normal mode anharmonicities and nonlinear couplings between the three coordinates. For the materials that I explored, polynomials with anharmonicities up to twentieth order and nonlinearities up to eighth order were needed to ensure accurate fit to the calculated energy surfaces. Since the polynomial fits the calculated energy surfaces almost exactly, there are no approximations in the calculations of the

nonlinear couplings, beyond that for the exchange-correlation functional.

The Born effective charges were calculated using density functional perturbation theory [32], and a larger $16 \times 16 \times 16$ $k$-point grid was used in these calculations. The calculated Born effective charges and phonon mode eigenvectors were used to calculate the mode effective charge $Z_m^*$ that determines the strength of the coupling of light to the pumped phonon mode from first principles [33]. The coupled equations of motion for the three coordinates were numerically solved using the LSODE subroutine of the OCTAVE software package [34].

### B. Identifying light-induced ferroelectricity

Phase transitions cannot occur at short timescales in nonequilibrium conditions, and any light-induced ferroelectricity will disappear once the external light source vanishes. Therefore, it is necessary to establish an unequivocal protocol for identifying light-induced ferroelectricity. Examining the intensity and phase of the second harmonic generation of the transmitted probe pulse is a convenient way to study ferroelectricity in pump-probe experiments [35,36], and it will be necessary to distinguish between light-induced ferroelectricity and a long-time-period excitation that both generate second harmonics if the probe pulse is shorter than the period of the low-frequency mode. For the purpose of this discussion, a light-induced ferroelectric state is deemed to have occurred both if the phase of the second harmonics does not change and the intensity of the second harmonics shows at least two peaks over the full width at half maximum (FWHM) duration of the pump pulse. Therefore the pump pulse duration should in general be larger than the period of the equilibrium-condition lowest frequency mode to establish light-induced ferroelectricity. However, this is not a strict condition, and other well-defined criteria could also be specified. In particular, the lowest frequency oscillations could (and indeed does) occur with a larger frequency in the rectified state, and any method (such as time resolved x-ray diffraction) that can distinguish oscillations about a displaced position can establish light-induced ferroelectricity.

## III. RESULTS AND DISCUSSIONS

### A. Cubic $KTaO_3$

The paraelectric phase of several $ABO_3$ perovskite oxides occurs in the cubic structure. So it is natural to ask if ferroelectricity can be induced in these cubic paraelectrics by a midinfrared excitation of their infrared-active phonon modes. These materials have five atoms per unit cell, and they thus have four triply degenerate optical phonon modes at the zone center. Factor group analysis shows that three of these modes have the irreducible representation $T_{1u}$, and these are infrared active. The remaining one has the irreducible representation $T_{2u}$ and is optically inactive. Ferroelectricity is generally ascribed to a dynamical instability of an infrared-active transverse optic phonon mode. Indeed, most ferroelectric materials show a characteristic softening of an infrared transverse optic mode as the transition temperature is approached [37]. Here I investigate if a similar softening and instability of the lowest frequency $T_{1u}$ mode can be
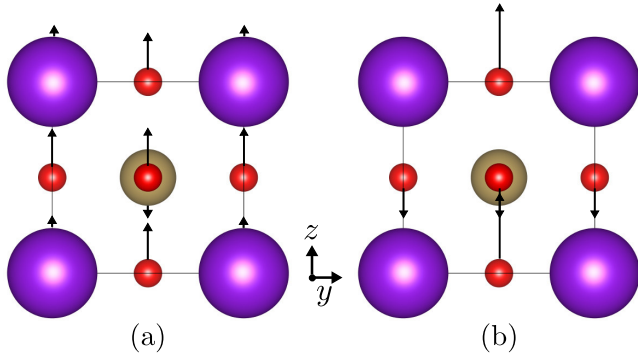
FIG. 1. Displacement patterns of the (a) lowest-frequency $Q_{1_z}$ and (b) highest-frequency $Q_{h_z}$ modes of the cubic phase of KTaO$_3$. The $x$ and $y$ components of these triply degenerate modes can be obtained by appropriate rotation. The big, medium, and small spheres denote K, Ta, and O, respectively.



FIG. 2. Total energy as a function of the longitudinal $Q_{1_x}$ coordinate for several values of the $Q_{h_x}$ coordinate for cubic KTaO$_3$.

achieved by an intense laser-induced excitation of the highest frequency $T_{1u}$ mode in the representative case of cubic KTaO$_3$. A related mechanism has been explored by Bousquet *et al.*, who have shown that a coupling between zone-center infrared and zone-boundary antiferrodistortive phonon modes can lead to improper ferroelectricity [38].

The calculated phonon frequencies of cubic KTaO$_3$ using the relaxed PBEsol lattice parameter of 3.99 Å are $\Omega_l = 85$ cm$^{-1}$ and $\Omega_h = 533$ cm$^{-1}$ for the lowest and highest frequency $T_{1u}$ modes, respectively. These are in good agreement with previously calculated values [39]. They also agree well with the frequencies obtained from hyper-Raman scattering experiments at room temperature [40]. The atomic displacement patterns due to these two modes are shown in Fig. 1. Without loss of generality, I consider the case where the $x$ component of the highest frequency $T_{1u}$ mode $Q_{h_x}$ is pumped by an intense light source and study how such an excitation changes the dynamics of the lowest frequency $T_{1u}$ mode along the longitudinal $Q_{1_x}$ and transverse $Q_{1_z}$ coordinates. I ignore the dynamics along the second transverse coordinate $Q_{1_y}$ as its dynamics will be qualitatively similar to that of the $Q_{1_z}$ coordinate.

### 1. Dynamics of the lowest frequency longitudinal component

Figure 2 shows several total energy $V(Q_{1_z}, Q_{1_x}, Q_{h_x})$ curves along the projection $Q_{1_z} = 0$. The curves are not symmetric upon reflection at $Q_{1_x} = 0$ and the $+Q_{h_x}$ and $-Q_{h_x}$ curves do not overlap. This indicates the presence of coupling terms that have odd orders of $Q_{1_x}$ and $Q_{h_x}$. A polynomial fit of the energy surface shows that the coupling terms $t_1 Q_{1_x}^3 Q_{h_x}$, $t_2 Q_{1_x}^2 Q_{h_x}^2$ and $t_3 Q_{1_x} Q_{h_x}^3$ are all large relative to the harmonic term $\Omega_l^2$ of the lowest frequency mode (see Table I). The presence of these couplings is consistent with the symmetry requirements. Since the equilibrium structure has inversion symmetry and we are considering two odd modes along the same direction, any term $Q_{1_x}^m Q_{h_x}^n$ is allowed as long as $m + n =$ even. The next allowed order of coupling is $Q_{1_x}^m Q_{h_x}^n$ with $m + n = 6$. These are an order of magnitude smaller than the $m + n = 4$ terms (see Table II in Appendix), but they are comparable in magnitude to the harmonic term $\Omega_l^2$.
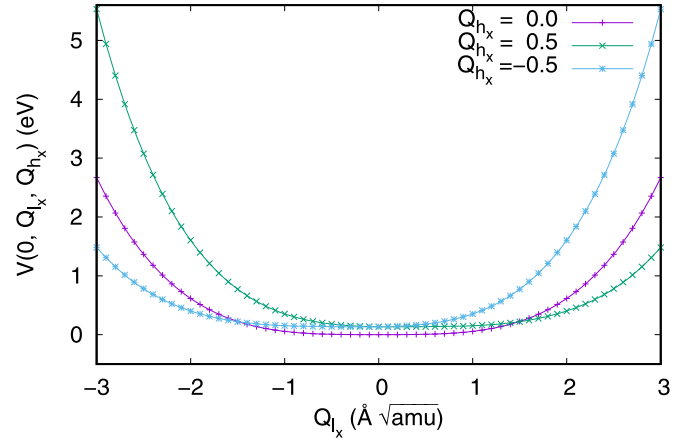
The nonlinear couplings between the $Q_{1_x}$ and $Q_{h_x}$ modes impart a force equal to $-\partial V/\partial Q_{1_x}$ along the $Q_{1_x}$ coordinate. This force is finite and large when the $Q_{h_x}$ mode is externally excited by an intense light source. The lowest-order nonlinear terms of this force are $-\partial V/\partial Q_{1_x} = -3t_1 Q_{1_x}^2 Q_{h_x} - 2t_2 Q_{1_x} Q_{h_x}^2 - t_3 Q_{h_x}^3$. The $-t_3 Q_{h_x}^3$ term acts as a nonresonant oscillating force to the $Q_{1_x}$ mode. The effect of the $-3t_1 Q_{1_x}^2 Q_{h_x}$ term would average over the slow oscillation of the $Q_{1_x}$ mode relative to that of the $Q_{h_x}$ mode. The $-2t_2 Q_{1_x} Q_{h_x}^2$ term affects a time-dependent modulation of the frequency of the $Q_{1_x}$ mode, and it does not cancel over the slow oscillation of the $Q_{1_x}$ mode because $Q_{h_x}^2$ has a nonzero time average [17,19]. Unfortunately, the sign of $t_2$ is positive, so the frequency of the $Q_{1_x}$ mode increases as the $Q_{h_x}$ mode is pumped. A similar analysis of the next order $Q_{1_x}^m Q_{h_x}^n$ terms with $m + n = 6$ also shows that the $Q_{1_x}$ mode does not soften due to the effects of nonlinear coupling terms.

### 2. Dynamics of the lowest frequency transverse component

What about the dynamics of the transverse component $Q_{1_z}$ of the lowest frequency mode? Figure 3 shows several total energy $V(Q_{1_z}, Q_{1_x}, Q_{h_x})$ curves along the projection $Q_{1_x} = 0$.

TABLE I. The coefficients of the harmonic and nonlinear coupling terms of cubic and strained KTaO$_3$. The units of a $Q^m Q^n$ term are meV Å$^{-(m+n)}$ amu$^{\frac{-(m+n)}{2}}$. The sign of the coupling is relevant only when the coordinates come with even powers.

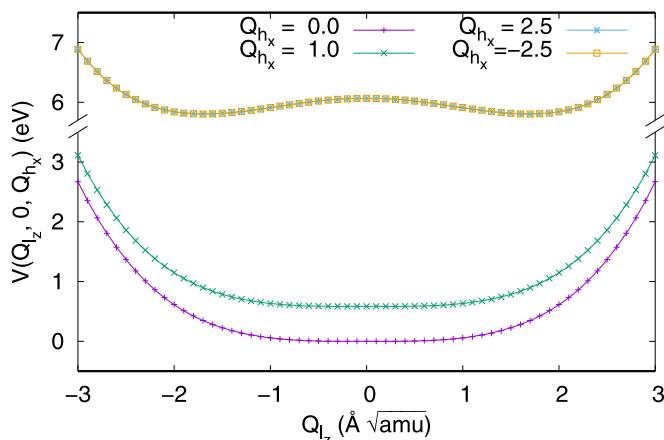| Coefficient | Order | Cubic | Strained |
|---|---|---|---|
| $\Omega_{1_z}^2$ | $Q_{1_z}^2$ | 27.06 | 1.39 |
| $\Omega_{1_x}^2$ | $Q_{1_x}^2$ | 27.06 | 55.27 |
| $\Omega_h^2$ | $Q_{h_x}^2$ | 1043.77 | 1136.10 |
| $t_1$ | $Q_{1_x}^3 Q_{h_x}$ | −118.35 | 97.38 |
| $t_2$ | $Q_{1_x}^2 Q_{h_x}^2$ | 215.00 | 208.76 |
| $t_3$ | $Q_{1_x} Q_{h_x}^3$ | −175.58 | 195.22 |
| $l$ | $Q_{1_z}^2 Q_{h_x}^2$ | −5.95 | −5.81 |
| $m_1$ | $Q_{1_z}^4 Q_{h_x}^2$ | −1.03 | −1.00 |
| $m_2$ | $Q_{1_z}^2 Q_{h_x}^4$ | −3.05 | −4.12 |

FIG. 3. Total energy as a function of the transverse $Q_{l_z}$ coordinate for several values of the $Q_{h_x}$ coordinate for cubic KTaO$_3$.

One immediately notices that the curves are symmetric upon reflection at $Q_{l_z} = 0$ and that the $-Q_{h_x}$ and $Q_{h_x}$ curves overlap, showing that only even powers of both $Q_{l_z}$ and $Q_{h_x}$ appear in the nonlinear coupling terms. This is again consistent with the symmetry requirements, which does not allow products with odd powers of mutually perpendicular components $Q_{l_z}$ and $Q_{h_x}$. The coefficients of the lowest-order nonlinear terms $l Q_{l_z}^2 Q_{h_x}^2$, $m_1 Q_{l_z}^4 Q_{h_x}^2$, and $m_2 Q_{l_z}^2 Q_{h_x}^4$ are given in Table I. They are all at least twenty times smaller than the magnitude of the quartic order couplings between the $Q_{l_x}$ and $Q_{h_x}$ coordinates. Nevertheless, the sign of the coupling coefficients between the $Q_{l_z}$ and $Q_{h_x}$ modes are such that these terms soften the frequency of the $Q_{l_z}$ mode, as one sees by analyzing the forcing terms due to these nonlinear couplings $-\partial V/\partial Q_{l_z} = -2l Q_{l_z} Q_{h_x}^2 - 4m_1 Q_{l_z}^3 Q_{h_x}^2 - 2m_2 Q_{l_z} Q_{h_x}^4$. Each term in the previous expression has even powers of the $Q_{h_x}$ coordinate, which ensures that their effects are not averaged over the slow oscillation of the $Q_{l_z}$ mode. Furthermore, all these terms are proportional to odd powers of the $Q_{l_z}$ coordinate, which causes the frequency of the $Q_{l_z}$ mode to change as $\Omega_{l_z}^2 \to \Omega_{l_z}^2 [1 + (2l Q_{h_x}^2(t) + 4m_1 Q_{l_z}^2(t) Q_{h_x}^2(t) + 2m_2 Q_{h_x}^4(t))/\Omega_{l_z}^2]$. Since the coupling constants are negative, this should lead to a softening of the transverse $Q_{l_z}$ mode when the $Q_{h_x}$ mode is externally pumped.

The above discussion is not sufficient to convincingly argue that the transverse $Q_{l_z}$ mode will become dynamically unstable when the $Q_{h_x}$ mode is externally pumped. There are two counteracting processes that may preclude this from happening. First, the coupling between the $Q_{l_x}$ and $Q_{h_x}$ modes is at least twenty times larger. As a result, the $Q_{l_z}$ component may receive a much smaller proportion of the external force due to nonlinear coupling with the $Q_{h_x}$ mode that is not sufficient to make this mode dynamically unstable when the latter is pumped. Moreover, I find that the coupling term $p Q_{l_z}^2 Q_{l_x}^2$ to be positive and larger than the term $l Q_{l_z}^2 Q_{h_x}^2$ (see Table II in Appendix). When the $Q_{l_x}$ component oscillates with a large amplitude, this will provide an additive factor that increases the frequency of the $Q_{l_z}$ component.

To settle this issue, I numerically solved the coupled equations of motion of the three coordinates $Q_{l_z}$, $Q_{l_x}$, and $Q_{h_x}$, which are

$$\ddot{Q}_{h_x} + \gamma_h \dot{Q}_{h_x} + \Omega_h^2 Q_{h_x} = -\frac{\partial V^{nh}(Q_{l_z}, Q_{l_x}, Q_{h_x})}{\partial Q_{h_x}} + F(t),$$

$$\ddot{Q}_{l_x} + \gamma_l \dot{Q}_{l_x} + \Omega_l^2 Q_{l_x} = -\frac{\partial V^{nh}(Q_{l_z}, Q_{l_x}, Q_{h_x})}{\partial Q_{l_x}},$$

$$\ddot{Q}_{l_z} + \gamma_l \dot{Q}_{l_z} + \Omega_l^2 Q_{l_z} = -\frac{\partial V^{nh}(Q_{l_z}, Q_{l_x}, Q_{h_x})}{\partial Q_{l_z}}. \quad (1)$$

Here, $V^{nh}(Q_{l_z}, Q_{l_x}, Q_{h_x})$ is the nonharmonic part of the polynomial that fits the calculated energy surface, and it includes both the anharmonicities of each coordinates as well as the nonlinear couplings between these coordinates. The full expression for $V^{nh}(Q_{l_z}, Q_{l_x}, Q_{h_x})$ is given in Eq. (A1) in Appendix. In addition to the numerically large nonlinear couplings discussed above, it includes anharmonicities up to the sixteenth-order and nonlinear couplings up to the eighth order. $\gamma_h$ and $\gamma_l$ are the damping coefficients of the highest and lowest frequency $T_{1u}$ modes, respectively. They are taken to be ten percent of the respective harmonic terms. $F(t) = Z_{h_x}^* E_0 \sin(\Omega t) e^{-t^2/2(\sigma/2\sqrt{2\ln 2})^2}$ is the external force experienced by the $Q_{h_x}$ coordinate due to a light pulse of peak electric field $E_0$. The calculated mode effective charge of the $Q_{h_x}$ mode of cubic KTaO$_3$ is $Z_{h_x}^* = -1.07e$ amu$^{-\frac{1}{2}}$. A pump with a frequency of $\Omega = 1.01\Omega_h$ and FWHM of $\sigma = 2.0$ ps has been used. The use of a long pulse width is just to illustrate many oscillation cycles. The physics does not change when I use a pulse duration larger than $1/\Omega_l$.

The result of the numerical integration of Eq. (1) in a highly nonlinear regime is shown in Fig. 4. This was obtained with a large peak electric field of $E_0 = 30$ MV cm$^{-1}$ that caused the pumped $Q_{h_x}$ mode to oscillate with a maximum amplitude of 1.1 Å$\sqrt{\text{amu}}$ [Fig. 4(b)]. In this regime, the $Q_{l_x}$ mode oscillates about the equilibrium position with a maximum amplitude of 0.25 Å$\sqrt{\text{amu}}$ (not shown). The frequency of its transverse counterpart $Q_{l_z}$ does soften by around ~5%. But relatively little force is imparted to the $Q_{l_z}$ component, and its oscillations about the equilibrium position are damped even during the duration of the pump pulse [Fig. 4(a)]. I performed similar calculations for pump fields up to 100 MV cm$^{-1}$ but was not able to find any instances where the $Q_{l_z}$ mode becomes dynamically unstable.

These calculations show that a dynamical instability of the lowest frequency infrared mode of cubic KTaO$_3$ cannot be achieved by a midinfrared excitation of its highest frequency infrared mode. However, this does not allow us to infer that light-induced dynamical instability cannot occur in any cubic paraelectric. Indeed, if I artificially increase the coefficient of the $l Q_{l_z}^2 Q_{h_x}^2$ term by six times, I am able to obtain a solution where the $Q_{l_z}$ coordinate oscillates about a displaced position during the duration of the pump pulse. Such a large coupling between the pumped high-frequency mode and the transverse component of the low-frequency mode may exist in some materials.

### B. Strained KTaO$_3$

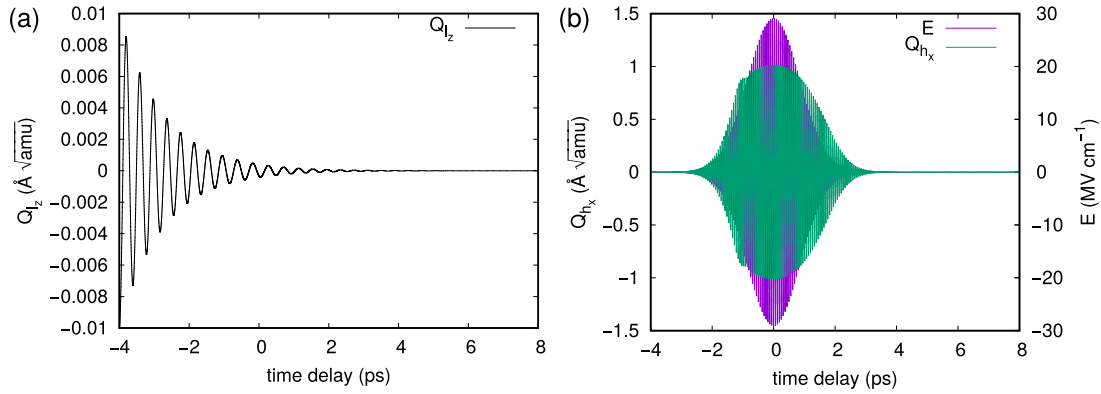If the coupling between the externally pumped highest frequency $T_{1u}$ mode and the component of the lowest

FIG. 4. Dynamics of the (a) $Q_{1_z}$ and (b) $Q_{h_x}$ coordinates of cubic KTaO$_3$ after the $Q_{h_x}$ coordinate is pumped by a pump pulse $E$ with FWHM of 2 ps as shown in (b).

frequency $T_{1u}$ mode longitudinal to the pumped mode could be weakened in cubic KTaO$_3$, the transverse component of the lowest frequency mode would develop a light-induced dynamical instability. An effective way of achieving this is by raising the frequency of the longitudinal component relative to that of the transverse component. This can be accomplished by applying a biaxial strain on KTaO$_3$ via an epitaxial growth on an appropriate substrate.

I performed calculations on KTaO$_3$ with 0.6% compressive biaxial strain. This can be achieved, for example, by growing KTaO$_3$ on a GdScO$_3$ substrate. The calculated PBEsol lattice parameters of thus strained KTaO$_3$ are $a = b = 3.965$ and $c = 4.0$ Å. Upon the application of a biaxial strain, the $T_{1u}$ mode of the cubic phase splits into a nondegenerate $A_{2u}$ mode and a doubly degenerate $E_u$ mode. The $A_{2u}$ phonons involve atomic motions along the $z$ axis while the atoms move in the $xy$ plane for the $E_u$ phonons. The calculated values for the lowest frequency $A_{2u}$ and $E_u$ modes are $\Omega_{1_z} = 20$ and $\Omega_{1_x} = \Omega_{1_y} = 122$ cm$^{-1}$, respectively. The highest frequency $E_u$ phonon that should be externally pumped has a frequency of $\Omega_{h} = 556$ cm$^{-1}$.

To find out whether the lowest frequency $A_{2u}$ mode $Q_{1_z}$ of strained KTaO$_3$ develops a dynamical instability when the $x$ component of the highest frequency $E_u$ mode $Q_{h_x}$ is intensely excited by a light source, I again started my investigation by calculating the total energy surface $V(Q_{1_z}, Q_{1_x}, Q_{h_x})$ as a function of the three coordinates using density functional calculations. The nonlinear couplings between the $Q_{1_z}$, $Q_{1_x}$, and $Q_{h_x}$ coordinates of strained KTaO$_3$ have the same symmetry requirements as discussed for the cubic case, and a fit of a general polynomial to the calculated first-principles $V(Q_{1_z}, Q_{1_x}, Q_{h_x})$ shows that same orders of nonlinearities are present in both the cases. As a comparison of the numbers presented in Table I shows (see also Table II in Appendix), the nonlinear couplings in the two cases do not differ by a large amount. The crucial difference between the two cases is that the frequencies of the $Q_{1_z}$ and $Q_{1_x}$ coordinates are different in the strained case ($\Omega_{1_z} = 20$ and $\Omega_{1_x} = 122$ cm$^{-1}$), whereas they are equal in the cubic case ($\Omega_{1_z} = \Omega_{1_x} = 85$ cm$^{-1}$). This has a profound effect in the dynamics of the $Q_{1_z}$ coordinate because the forces experienced by a coordinate due to the nonlinear couplings are weighted by the square of the frequency of the coordinate. We can see that $\frac{1}{20^2} \frac{\partial V}{\partial Q_{1_z}}$ is likely to be much larger

than $\frac{1}{122^2} \frac{\partial V}{\partial Q_{1_x}}$ or $\frac{1}{85^2} \frac{\partial V}{\partial Q_{1_x}}$. In simple words, the $Q_{1_z}$ coordinate of strained KTaO$_3$ gets much larger proportion of the force than the $Q_{1_z}$ coordinate of cubic KTaO$_3$ because the frequency of the $Q_{1_z}$ mode is much smaller in the strained structure compared to the cubic structure. Is this change big enough to result in a light-induced dynamical instability of the $Q_{1_z}$ mode in strained KTaO$_3$?

I again solved the coupled equations of motion of the three coordinates $Q_{h_x}$, $Q_{1_x}$, and $Q_{1_z}$ as given by Eq. (1) for the case of strained KTaO$_3$. This time I used the potential $V^{nh}(Q_{1_z}, Q_{1_x}, Q_{h_x})$ obtained for strained KTaO$_3$ from first principles. The polynomial expression used in the calculations and the numerical values of the coefficients for all the terms in the polynomial that fit the calculated energy surface are given in Appendix. A pump pulse with an FWHM of 2 ps ($> 1/\Omega_{1_z}$) and frequency $1.01\Omega_h$ is again used to excite the $Q_{h_x}$ mode. The mode effective charge of the $Q_{h_x}$ mode in the strained structure is $Z^*_{h_x} = -1.15e$ amu$^{-\frac{1}{2}}$.

Figure 5 shows the results of the numerical integration of these equations for three different regimes of dynamics of the $Q_{1_z}$ coordinate. At relatively small peak electric fields of the pump ($E_0 < 1$ MV cm$^{-1}$), the $Q_{1_z}$ mode oscillates about the equilibrium position with its harmonic frequency (not shown). As the peak electric field is increased, the frequency of the $Q_{1_z}$ mode decreases during the duration that the $Q_{h_x}$ mode is being pumped [Fig. 5(a)]. As discussed above, this is due to the negative values of the coefficients of the coupling terms $l Q_{1_z}^2 Q_{h_x}^2$, $m_1 Q_{1_z}^4 Q_{h_x}^2$, and $m_2 Q_{1_z}^2 Q_{h_x}^4$ that cause a light-induced softening of the $Q_{1_z}$ coordinate. Since the duration of the pump pulse is finite, I naturally do not observe the period of the $Q_{1_z}$ mode diverge. Instead, beyond a critical value of the peak electric field of the pump ($E_0^c \simeq 17$ MV cm$^{-1}$ for $\sigma = 2$ ps), the $Q_{1_z}$ coordinate oscillates about a displaced position and has a nonzero value while the $Q_{h_x}$ mode is being pumped [Figs. 5(b) and 5(c)]. In this rectified regime, the average potential felt by the $Q_{1_z}$ mode has a double-well structure, and this mode is oscillating about one of the minima. The displacement along the $Q_{1_z}$ coordinate is also amplified strongly in this regime. Since the $Q_{1_z}$ mode is infrared active, this implies that the material is in a broken symmetry state with a finite dipole moment while the $Q_{h_x}$ mode is externally pumped.
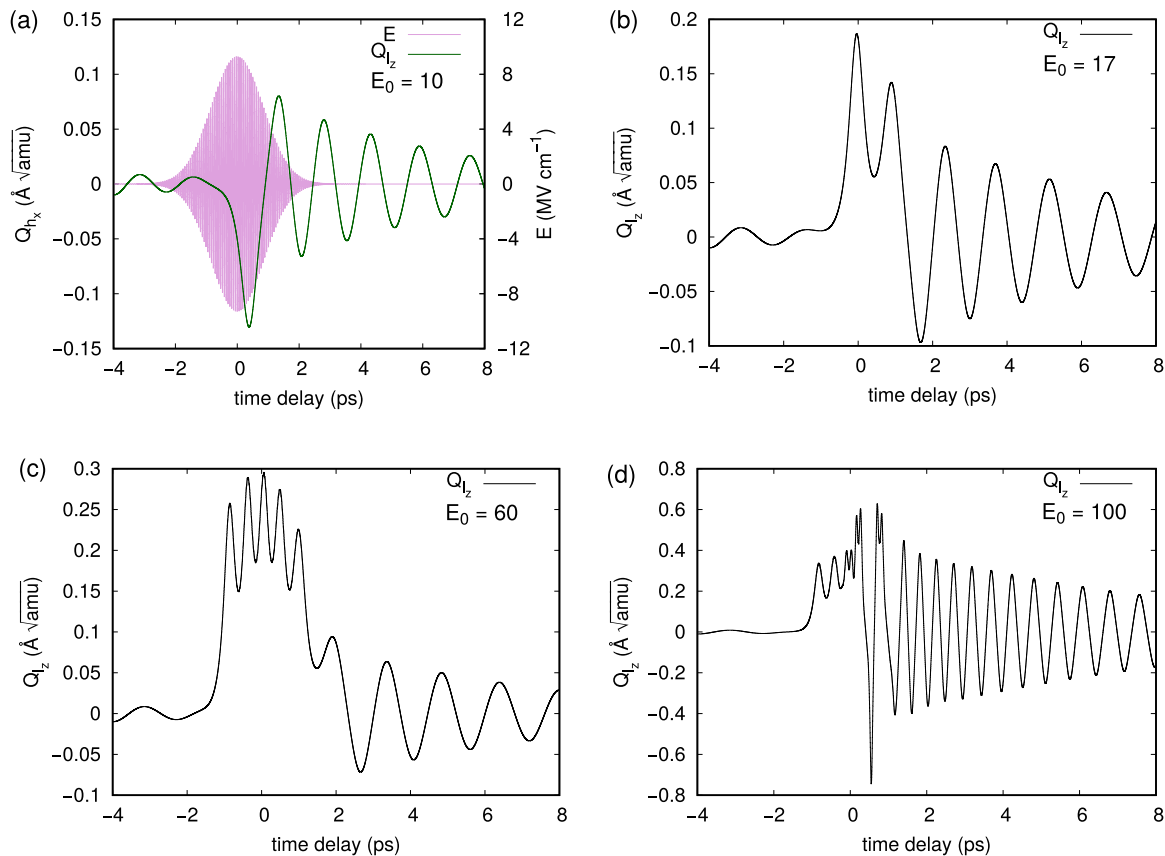
FIG. 5. Dynamics of the $Q_{1_z}$ coordinate of strained KTaO$_3$ after the $Q_{h_x}$ coordinate is pumped by a pump pulse $E$ with FWHM of 2 ps. The dynamics for four different values of the peak electric field $E_0$ (MV cm$^{-1}$) of the pump pulse are shown.

The frequency of the $Q_{1_z}$ oscillations in the rectified state increases as the peak electric field of the pump is increased beyond the critical threshold. This is evident from a comparison of Figs. 5(b) and 5(c), which shows that the frequency of the $Q_{1_z}$ mode doubles as the peak electric field $E_0$ is increased from 17 to 60 MV cm$^{-1}$. This increase occurs because the double-well potential for the $Q_{1_z}$ coordinate becomes deeper as the amplitude of the $Q_{h_x}$ oscillations increases.

When the peak electric field is increased further ($E_0 > 75$ MV cm$^{-1}$), the $Q_{1_z}$ mode oscillates with a large amplitude and high frequency about the equilibrium position [Fig. 5(d)]. In this regime, the kinetic energy imparted to the $Q_{1_z}$ mode is larger than the depth of the double wells. As a result, the oscillation of the $Q_{1_z}$ mode stops being confined to one of the double wells, and the rectified behavior along the $Q_{1_z}$ coordinate is no longer observed. Even though the light-induced broken-symmetry phase is stabilized only for a range of values of the peak electric field of the pump, this range $17 < E_0 < 75$ MV cm$^{-1}$ is both wide and approachable enough to make the light-induced ferroelectric state experimentally accessible.

The existence of a critical threshold above which the $Q_{1_z}$ coordinate is rectified and the presence of three different regimes for the dynamics of this coordinate is consistent with the analysis of a $Q_1^2 Q_2^2$ nonlinear coupling between two different normal mode coordinates as presented in Ref. [19]. These features should be present in the experiments to confirm

the predictions made in this work. The critical pump amplitude depends on the frequencies of the $Q_{1_z}$ and $Q_{h_x}$ modes and the coupling coefficient, as well as the pump pulse length and the initial condition (i.e., the root mean square displacement of the $Q_{1_z}$ mode at a particular temperature) [19]. For a pump pulse with FWHM of 2 ps, I find that the $Q_{1_z}$ mode starts to get rectified when the peak electric field is $E_0 = 17$ MV cm$^{-1}$. With this pump pulse, the $Q_{h_x}$ mode is oscillating with an amplitude of 0.9 Å$\sqrt{\text{amu}}$, which corresponds to a maximum change in the Ta-apical O bond length of 0.2 Å (that is, 10%). The $Q_{h_x}$ mode oscillates with an amplitude of 1.3 Å$\sqrt{\text{amu}}$ when the peak electric field is increased to $E_0 = 75$ MV cm$^{-1}$. This is a modest increase in the energy of the $Q_{h_x}$ mode due to the pump, and it indicates that a significant fraction of the pumped energy goes to maintaining the rectified state along the $Q_{1_z}$ coordinate. However, the light-induced ferroelectric displacement along the $Q_{1_z}$ coordinate is quite small because of the small magnitude of the couplings between $Q_{1_z}$ and $Q_{h_x}$ modes. The average displacement along $Q_{1_z}$ is ~0.1 and ~0.2 Å$\sqrt{\text{amu}}$ for $E_0 = 17$ and 75 MV cm$^{-1}$, respectively, which results in the change of Ta-apical O distance by 0.015–0.030 Å.

Curiously, the critical pump threshold obtained for strained KTaO$_3$ is noticeably smaller than what is expected for a $Q_{1_z}^2 Q_{h_x}^2$ coupling. In the total energy calculations, the $Q_{1_z}$ mode starts developing instability when $Q_{h_x}$ is above 0.7 Å$\sqrt{\text{amu}}$. So the critical $Q_{h_x}$ amplitude should be $0.7\sqrt{2} = 1.0$ Å$\sqrt{\text{amu}}$ [19].
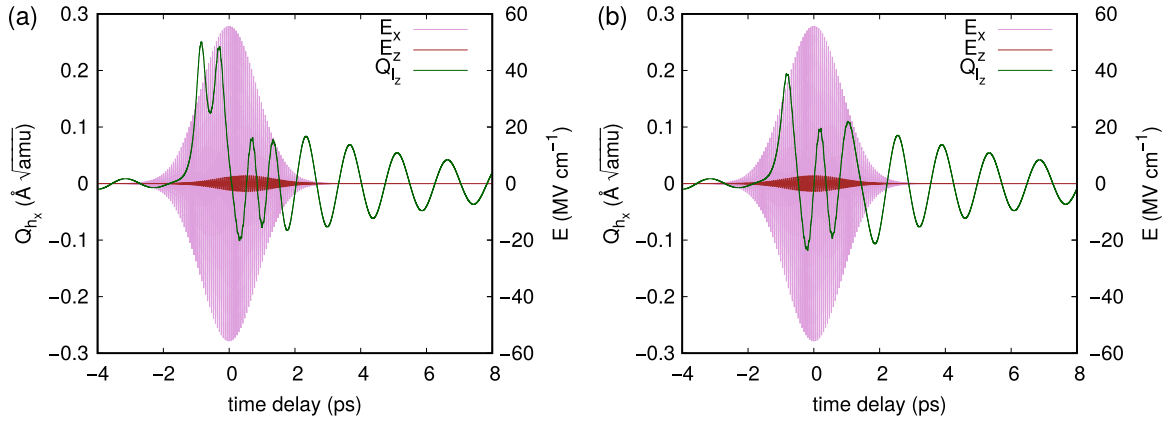
FIG. 6. Dynamics of the $Q_{l_z}$ coordinate of strained KTaO$_3$ for the delays of (a) 0.5 and (b) 0.0 ps between the $E_{h_x}$ and $E_{h_z}$ pulses that pump $Q_{h_x}$ and $Q_{h_z}$ modes, respectively.

Instead, I find that the $Q_{l_z}$ mode becomes unstable when the $Q_{h_x}$ amplitude is 0.9 Å$\sqrt{\text{amu}}$. This reduction in the critical threshold is due to the presence of a large and negative sixth-order coupling terms $m_1 Q_{l_z}^4 Q_{h_x}^2$ and $m_2 Q_{l_z}^2 Q_{h_x}^4$. Both these terms give a subtractive contribution to the effective, light-induced frequency of the $Q_{l_z}$ mode, which hastens its instability as a function of the pump intensity.

### C. Abruptly halting light-induced ferroelectricity

For light-induced ferroelectricity to be useful in applications, it is necessary to be able to control the light-induced phase at will in an all-optical setup. In this context, this means having the capability to switch off the rectification of the $Q_{l_z}$ mode while the $Q_{h_x}$ mode is being pumped. The quartic order odd $Q_{l_z}^3 Q_{h_z}$ and $Q_{l_z} Q_{h_z}^3$ couplings in the longitudinal direction can be used to our advantage for this purpose. To investigate this possibility, I consider an experiment where an overlapping pulse polarized along $Q_{h_z}$ comes at an arbitrary delay with respect to the rectification-causing pulse that pumps the $Q_{h_x}$ mode. I study the resulting dynamics along the $Q_{l_z}$ coordinate by solving the coupled equations of motion for the four coordinates ($Q_{l_z}, Q_{l_x}, Q_{h_x}$, and $Q_{h_z}$). The equations of motions are obtained from the potential $V^{\text{nh}}(Q_{l_z}, Q_{l_x}, Q_{h_x}) + V^{\text{nh}}(Q_{l_z}, Q_{h_z})$. For computational efficiency, I do not consider the full potential $V^{\text{nh}}(Q_{l_z}, Q_{l_x}, Q_{h_x}, Q_{h_x})$ spanned by the four coordinates.

The results for the delays of 0.5 and 0.0 ps between the pump pulses $E_{h_x}$ and $E_{h_z}$ that excite the $Q_{h_x}$ and $Q_{h_z}$ coordinates, respectively, are shown in Fig. 6. The peak electric fields of $E_{h_x}$ and $E_{h_z}$ are 60 and 3 MV cm$^{-1}$, respectively, and their FWHM is 2 ps. The pump frequencies are 1.01 times the respective phonon frequencies, and the mode effective charge of $Q_{h_z}$ is $Z_{h_z}^* = -1.05e$ amu$^{-\frac{1}{2}}$. Note that excitation by only $E_{h_x}$ causes rectification of the $Q_{l_z}$ mode during the FWHM of the pulse [Fig. 5(c)]. However, an overlapping excitation by another weak pulse $E_{h_z}$ immediately suppresses the light-induced rectification of the $Q_{l_z}$ mode. Even a weak longitudinal pump is efficient in halting the rectification because the quartic order odd couplings between $Q_{l_z}$ and $Q_{h_z}$ modes are much larger than the couplings in the transverse direction.

## IV. SUMMARY AND CONCLUSIONS

In summary, I have shown that midinfrared pulses can be used to stabilize nonequilibrium ferroelectricity in strained KTaO$_3$, which is paraelectric at equilibrium conditions. This phenomenon relies on a quartic $l Q_{l_z}^2 Q_{h_x}^2$ coupling between the highest frequency infrared-active phonon mode $Q_{h_x}$ and the lowest frequency infrared-active mode $Q_{l_z}$ that is transverse to $Q_{h_x}$. Density functional calculations show that the coupling constant $l$ is negative, which causes the $Q_{l_z}$ mode to soften when the $Q_{h_x}$ mode is externally pumped. The rectification along the $Q_{l_z}$ coordinate occurs only above a critical electric field of the pump pulse, demonstrating that this light-induced symmetry breaking is a unique nonperturbative effect. Such a threshold behavior should be observed in experiments to corroborate the predictions made in this paper. Additionally, the $Q_{l_z}^4 Q_{h_x}^2$ and $Q_{l_z}^2 Q_{h_x}^4$ couplings are large, and this makes the rectified regime more accessible. A first-principles calculation of the coupling between light and the $Q_{h_x}$ mode shows that ferroelectricity can be induced in strained KTaO$_3$ by a midinfrared pulse with a peak electric field of 17 MV cm$^{-1}$ and a duration of 2 ps. Furthermore, large odd quartic couplings $Q_{l_z}^3 Q_{h_z}$ and $Q_{l_z} Q_{h_z}^3$ between $Q_{l_z}$ and the highest frequency infrared-active mode $Q_{h_z}$ longitudinal to $Q_{l_z}$ makes it possible to arbitrarily switch off the induced ferroelectricity by pumping the $Q_{h_z}$ mode with another weak pulse. I find that similar nonlinear interactions exist in SrTiO$_3$ and LaAlO$_3$, and this technique could be generally applied to other transition metal oxide paraelectrics.

At a more basic level, I have shown that materials can exhibit various nonlinear interactions between different dynamical degrees of freedom that have hitherto been over-looked. These interactions enable us to induce and control broken-symmetry phases using light, whose oscillating electric and magnetic fields average to zero by definition. Furthermore, I have demonstrated that the nonlinear interactions can be effectively modified by applying strain. This motivates experiments that combine the disparate fields of nonlinear optics and heterostructuring to achieve materials control in an interesting manner. In a broader perspective, these nonlinear interactions may also be present in other classes of systems, and they might allow us to influence the dynamics of these systems in an unusual way.

## APPENDIX A: EXPRESSIONS FOR TOTAL ENERGY SURFACES

Only low-order nonlinear couplings that are relatively large were discussed in the main text. However, if only low-order couplings and anharmonicities are considered, the fit to the calculated total-energy surfaces are not satisfactory. The dynamics of the coordinates with and without using the high-order couplings also show large differences, especially at the nonlinear regime. Since the use of the full polynomial expression in the solutions of the equations of motion are not computationally demanding, all the numerical results discussed in this paper were obtained using the full expression given below.

For cubic KTaO$_3$, the following polynomial $V(Q_{1_z}, Q_{1_x}, Q_{h_x})$ accurately fits the calculated total energy surface spanned by the three coordinates for values between $-3.0$ and $3.0$ Å$\sqrt{\text{amu}}$:

$$
\begin{aligned}
V = {} & \tfrac{1}{2}\Omega_1^2 Q_{1_z}^2 + a_4 Q_{1_z}^4 + a_6 Q_{1_z}^6 + a_8 Q_{1_z}^8 + a_{10} Q_{1_z}^{10} \\
& + a_{12} Q_{1_z}^{12} + a_{14} Q_{1_z}^{14} + a_{16} Q_{1_z}^{16} + \tfrac{1}{2}\Omega_1^2 Q_{1_x}^2 + a_4 Q_{1_x}^4 \\
& + a_6 Q_{1_x}^6 + a_8 Q_{1_x}^8 + a_{10} Q_{1_x}^{10} + a_{12} Q_{1_x}^{12} + a_{14} Q_{1_x}^{14} \\
& + a_{16} Q_{1_x}^{16} + \tfrac{1}{2}\Omega_h^2 Q_{h_x}^2 + c_4 Q_{h_x}^4 + c_6 Q_{h_x}^6 + c_8 Q_{h_x}^8 \\
& + c_{10} Q_{h_x}^{10} + c_{12} Q_{h_x}^{12} + l Q_{1_z}^2 Q_{h_x}^2 + m_1 Q_{1_z}^4 Q_{h_x}^2 \\
& + m_2 Q_{1_z}^2 Q_{h_x}^4 + n_1 Q_{1_z}^4 Q_{h_x}^4 + n_2 Q_{1_z}^6 Q_{h_x}^2 + n_3 Q_{1_z}^2 Q_{h_x}^6 \\
& + t_1 Q_{1_x}^3 Q_{h_x} + t_2 Q_{1_x}^2 Q_{h_x}^2 + t_3 Q_{1_x} Q_{h_x}^3 + u_1 Q_{1_x}^5 Q_{h_x} \\
& + u_2 Q_{1_x}^4 Q_{h_x}^2 + u_3 Q_{1_x}^3 Q_{h_x}^3 + u_4 Q_{1_x}^2 Q_{h_x}^4 + u_5 Q_{1_x} Q_{h_x}^5 \\
& + p Q_{1_z}^2 Q_{1_x}^2 + q_1 Q_{1_z}^4 Q_{1_x}^2 + q_2 Q_{1_z}^2 Q_{1_x}^4 + r_1 Q_{1_z}^4 Q_{1_x}^4 \\
& + r_2 Q_{1_z}^6 Q_{1_x}^2 + r_3 Q_{1_z}^2 Q_{1_x}^6 + d Q_{1_z}^2 Q_{1_x} Q_{h_x} \\
& + e_1 Q_{1_z}^2 Q_{1_x}^3 Q_{h_x} + e_2 Q_{1_z}^2 Q_{1_x}^2 Q_{h_x}^2 + e_3 Q_{1_z}^2 Q_{1_x} Q_{h_x}^3 \\
& + f_1 Q_{1_z}^2 Q_{1_x}^5 Q_{h_x} + f_2 Q_{1_z}^2 Q_{1_x}^4 Q_{h_x}^2 + f_3 Q_{1_z}^2 Q_{1_x}^3 Q_{h_x}^3 \\
& + f_4 Q_{1_z}^2 Q_{1_x}^2 Q_{h_x}^4 + f_5 Q_{1_z}^2 Q_{1_x} Q_{h_x}^5 + g Q_{1_z}^4 Q_{1_x} Q_{h_x} \\
& + h_1 Q_{1_z}^4 Q_{1_x}^3 Q_{h_x} + h_2 Q_{1_z}^4 Q_{1_x}^2 Q_{h_x}^2 + h_3 Q_{1_z}^4 Q_{1_x} Q_{h_x}^3.
\end{aligned}
\tag{A1}
$$

For strained KTaO$_3$, the potential has additional $a_{18} Q_{1_z}^{18}$ and $a_{20} Q_{1_z}^{20}$ terms. Also, the coefficients of the $Q_{1_z}^n$ and $Q_{1_x}^n$ terms are different in the strained case. The coefficients of the $Q_{1_x}^n$ terms for the strained case are denoted by $b_n$ in Table II.

The polynomial $V(Q_{1_z}, Q_{h_z})$ that fits the energy surface spanned by the $Q_{1_z}$ and $Q_{h_z}$ coordinates is given by

$$
\begin{aligned}
V = {} & \tfrac{1}{2}\Omega_{1_z}^2 Q_{1_z}^2 + a_4 Q_{1_z}^4 + a_6 Q_{1_z}^6 + a_8 Q_{1_z}^8 + a_{10} Q_{1_z}^{10} \\
& + a_{12} Q_{1_z}^{12} + a_{14} Q_{1_z}^{14} + a_{16} Q_{1_z}^{16} + a_{18} Q_{1_z}^{18} + a_{20} Q_{1_z}^{20}
\end{aligned}
$$

$$
\begin{aligned}
& + \tfrac{1}{2}\Omega_{h_z}^2 Q_{h_z}^2 + d_4 Q_{h_z}^4 + d_6 Q_{h_z}^6 + d_8 Q_{h_z}^8 + d_{10} Q_{h_z}^{10} \\
& + d_{12} Q_{h_z}^{12} + v_1 Q_{1_z}^3 Q_{h_z} + v_2 Q_{1_z}^2 Q_{h_z}^2 + v_3 Q_{1_z} Q_{h_z}^3 \\
& + w_1 Q_{1_z}^5 Q_{h_z} + w_2 Q_{1_z}^4 Q_{h_z}^2 + w_3 Q_{1_z}^3 Q_{h_z}^3 + w_4 Q_{1_z}^2 Q_{h_z}^4 \\
& + w_5 Q_{1_z} Q_{h_z}^5.
\end{aligned}
\tag{A2}
$$

The nonharmonic potential $V^{\text{nh}}$ defined in the main text is $V$ without the harmonic $\tfrac{1}{2}\Omega Q^2$ terms. The values of all the coefficients in Eqs. (A1) and (A2) obtained from a fit to the calculated energy surfaces of cubic and strained KTaO$_3$ are given in Table II. I note that values lower than the magnitude of $10^{-5}$ are below the accuracy of the density functional calculations. They are kept so that that the highest-order anharmonicity has a positive sign, which keeps the numerical solution of the equation of motions stable.

## APPENDIX B: MODE EFFECTIVE CHARGES

The mode effective charge vector $Z_{m,\alpha}^* = \partial F_{m,\alpha}/\partial E_\alpha$ relates the force $F_{m,\alpha}$ experienced by the normal mode coordinate $Q_m$ due to an electric field $E_\alpha$ along the direction $\alpha$. It is related to the Born effective charges $Z_{\kappa,\alpha\beta}^*$ of atoms $\kappa$ in the unit cell of a material by [33]

$$
Z_{m,\alpha}^* = \sum_{\kappa,\beta} Z_{\kappa,\alpha\beta}^* U_m(\kappa,\beta),
$$

where $U_m(\kappa,\beta)$ is the $\mathbf{q} = 0$ eigendisplacement vector normalized as

$$
\sum_{\kappa,\beta} M_\kappa [U_m(\kappa,\beta)]^* U_n(\kappa,\beta) = \delta_{mn}.
$$

Here, $M_\kappa$ is the mass of the atom $\kappa$. The eigendisplacement vector is related to the eigenvector $w_m(\kappa,\beta)$ of the dynamical matrix by

$$
U_m(\kappa,\beta) = \frac{w_m(\kappa,\beta)}{\sqrt{M_\kappa}}.
$$

Note that this definition of the mode effective charge is slightly different from the one used in Ref. [33]. Here, $Z_{m,\alpha}^*$ is related to the change in the value of the normal mode coordinate rather than the change in the atomic displacements due to a motion along the normal mode coordinate. This gives a different normalization factor for $Z_{m,\alpha}^*$, and this quantity is expressed in the units of $e$ amu$^{-\frac{1}{2}}$. Its sign is arbitrary because the eigenvector of the dynamical matrix is defined up to a multiplicative constant.

The mode effective charge can be experimentally determined. It is related to the ionic contribution to the dielectric constant by [33]

$$
\epsilon_{\alpha\beta}(\Omega) = \epsilon_{\alpha\beta}^\infty + \frac{4\pi}{V_0} \sum_m \frac{Z_{m,\alpha}^* Z_{m,\beta}^*}{\Omega_m^2 - \Omega^2},
$$

where $V_0$ is the unit cell volume and $\Omega_m$ is the frequency of the mode $m$. This expression shows that the oscillator strength measured in optical spectroscopy is the square of the mode effective charge.

TABLE II. The coefficients of the harmonic, anharmonic, and nonlinear coupling terms of cubic and strained KTaO$_3$. The units of a $Q^m Q^n Q^p$ term are meV Å$^{-(m+n+p)}$ amu$^{\frac{-(m+n+p)}{2}}$. The sign of the coupling is relevant only when the coordinates come with even powers.

| Coefficient | Order | Cubic | Strained |
|---|---|---|---|
| $\Omega^2_{l_z}$ | $Q^2_{l_z}$ | 27.06 | 1.39 |
| $\Omega^2_{l_x}$ | $Q^2_{l_x}$ | 27.06 | 55.27 |
| $\Omega^2_{h}$ | $Q^2_{h_x}$ | 1043.77 | 1136.10 |
| $a_4$ | $Q^4_{l_z}$ | 47.55 | 51.72 |
| $a_6$ | $Q^6_{l_z}$ | $-6.45$ | $-8.69$ |
| $a_8$ | $Q^8_{l_z}$ | 1.47 | 2.73 |
| $a_{10}$ | $Q^{10}_{l_z}$ | $-2.35 \times 10^{-1}$ | $-6.91 \times 10^{-1}$ |
| $a_{12}$ | $Q^{12}_{l_z}$ | $2.43 \times 10^{-2}$ | $1.28 \times 10^{-1}$ |
| $a_{14}$ | $Q^{14}_{l_z}$ | $-1.41 \times 10^{-3}$ | $-1.61 \times 10^{-2}$ |
| $a_{16}$ | $Q^{16}_{l_z}$ | $3.47 \times 10^{-5}$ | $1.30 \times 10^{-3}$ |
| $a_{18}$ | $Q^{18}_{l_z}$ | | $-6.04 \times 10^{-5}$ |
| $a_{20}$ | $Q^{20}_{l_z}$ | | $1.23 \times 10^{-6}$ |
| $c_4$ | $Q^4_{h_x}$ | 63.17 | 78.60 |
| $c_6$ | $Q^6_{h_x}$ | $-7.33 \times 10^{-1}$ | $-1.00$ |
| $c_8$ | $Q^8_{h_x}$ | $4.38 \times 10^{-1}$ | 7.22 |
| $c_{10}$ | $Q^{10}_{h_x}$ | $-1.68 \times 10^{-2}$ | $-3.79 \times 10^{-2}$ |
| $c_{12}$ | $Q^{12}_{h_x}$ | $1.29 \times 10^{-4}$ | $6.49 \times 10^{-4}$ |
| $l$ | $Q^2_{l_z}Q^2_{h_x}$ | $-5.95$ | $-5.81$ |
| $m_1$ | $Q^4_{l_z}Q^2_{h_x}$ | $-1.03$ | $-1.00$ |
| $m_2$ | $Q^2_{l_z}Q^4_{h_x}$ | $-3.05$ | $-4.12$ |
| $n_1$ | $Q^4_{l_z}Q^4_{h_x}$ | $1.85 \times 10^{-1}$ | $2.41 \times 10^{-1}$ |
| $n_2$ | $Q^6_{l_z}Q^2_{h_x}$ | $4.35 \times 10^{-3}$ | 0.00 |
| $n_3$ | $Q^2_{l_z}Q^6_{h_x}$ | $-2.37 \times 10^{-1}$ | $-3.14 \times 10^{-1}$ |
| $t_1$ | $Q^3_{l_x}Q_{h_x}$ | $-118.35$ | 97.38 |
| $t_2$ | $Q^2_{l_x}Q^2_{h_x}$ | 215.00 | 208.76 |
| $t_3$ | $Q_{l_x}Q^3_{h_x}$ | $-175.58$ | 195.22 |
| $u_1$ | $Q^5_{l_x}Q_{h_x}$ | $-2.72$ | 1.73 |
| $u_2$ | $Q^4_{l_x}Q^2_{h_x}$ | 10.64 | 6.93 |
| $u_3$ | $Q^3_{l_x}Q^3_{h_x}$ | $-22.81$ | 18.34 |
| $u_4$ | $Q^2_{l_x}Q^4_{h_x}$ | 25.38 | 24.27 |
| $u_5$ | $Q_{l_x}Q^5_{h_x}$ | $-13.70$ | 15.57 |
| $p$ | $Q^2_{l_z}Q^2_{l_x}$ | 6.29 | 6.02 |
| $q_1$ | $Q^4_{l_z}Q^2_{l_x}$ | $-1.70$ | $-1.56$ |
| $q_2$ | $Q^2_{l_z}Q^4_{l_x}$ | $-1.70$ | $-1.39$ |
| $r_1$ | $Q^4_{l_z}Q^4_{l_x}$ | $9.35 \times 10^{-2}$ | $7.39 \times 10^{-2}$ |
| $r_2$ | $Q^6_{l_z}Q^2_{l_x}$ | $5.23 \times 10^{-3}$ | $7.12 \times 10^{-3}$ |
| $r_3$ | $Q^2_{l_z}Q^6_{l_x}$ | $5.23 \times 10^{-3}$ | $1.45 \times 10^{-2}$ |
| $d$ | $Q^2_{l_z}Q_{l_x}Q_{h_x}$ | $-19.09$ | 15.02 |
| $e_1$ | $Q^2_{l_z}Q^3_{l_x}Q_{h_x}$ | 6.61 | $-5.5$ |
| $e_2$ | $Q^2_{l_z}Q^2_{l_x}Q^2_{h_x}$ | $-13.16$ | $-13.62$ |
| $e_3$ | $Q^2_{l_z}Q_{l_x}Q^3_{h_x}$ | 11.32 | $-13.03$ |
| $f_1$ | $Q^2_{l_z}Q^5_{l_x}Q_{h_x}$ | $2.99 \times 10^{-1}$ | $-2.06 \times 10^{-1}$ |
| $f_2$ | $Q^2_{l_z}Q^4_{l_x}Q^2_{h_x}$ | $-6.80 \times 10^{-1}$ | $-4.44 \times 10^{-1}$ |
| $f_3$ | $Q^2_{l_z}Q^3_{l_x}Q^3_{h_x}$ | 1.39 | $-1.10$ |
| $f_4$ | $Q^2_{l_z}Q^2_{l_x}Q^4_{h_x}$ | $-1.45$ | $-1.34$ |
| $f_5$ | $Q^2_{l_z}Q_{l_x}Q^5_{h_x}$ | $8.75 \times 10^{-1}$ | $-9.52 \times 10^{-1}$ |
| $g$ | $Q^4_{l_z}Q_{l_x}Q_{h_x}$ | 1.02 | $-4.06 \times 10^{-1}$ |
| $h_1$ | $Q^4_{l_z}Q^3_{l_x}Q_{h_x}$ | $-4.62 \times 10^{-1}$ | $3.31 \times 10^{-1}$ |
| $h_2$ | $Q^4_{l_z}Q^2_{l_x}Q^2_{h_x}$ | $8.13 \times 10^{-1}$ | $7.51 \times 10^{-1}$ |
| $h_3$ | $Q^4_{l_z}Q_{l_x}Q^3_{h_x}$ | $-7.45 \times 10^{-1}$ | $7.51 \times 10^{-1}$ |

| Coefficient | Order | Strained |
|---|---|---|
| $\Omega^2_{h_z}$ | $Q^2_{h_z}$ | 1034.38 |
| $b_4$ | $Q^4_{l_x}$ | 36.56 |
| $b_6$ | $Q^6_{l_x}$ | $-5.05$ |
| $b_8$ | $Q^8_{l_x}$ | 1.12 |
| $b_{10}$ | $Q^{10}_{l_x}$ | $-1.79 \times 10^{-1}$ |
| $b_{12}$ | $Q^{12}_{l_x}$ | $1.85 \times 10^{-2}$ |
| $b_{14}$ | $Q^{14}_{l_x}$ | $-1.07 \times 10^{-3}$ |
| $b_{16}$ | $Q^{16}_{l_x}$ | $2.64 \times 10^{-5}$ |
| $d_4$ | $Q^4_{h_z}$ | 61.23 |
| $d_6$ | $Q^6_{h_z}$ | $-7.24 \times 10^{-1}$ |
| $d_8$ | $Q^8_{h_z}$ | $3.97 \times 10^{-1}$ |
| $d_{10}$ | $Q^{10}_{h_z}$ | $-1.38 \times 10^{-2}$ |
| $d_{12}$ | $Q^{12}_{h_z}$ | $5.99 \times 10^{-5}$ |
| $v_1$ | $Q^3_{l_z}Q_{h_z}$ | 119.42 |
| $v_2$ | $Q^2_{l_z}Q^2_{h_z}$ | 212.45 |
| $v_3$ | $Q_{l_z}Q^3_{h_z}$ | 169.37 |
| $w_1$ | $Q^5_{l_z}Q_{h_z}$ | 2.88 |
| $w_2$ | $Q^4_{l_z}Q^2_{h_z}$ | 11.23 |
| $w_3$ | $Q^3_{l_z}Q^3_{h_z}$ | 23.54 |
| $w_4$ | $Q^2_{l_z}Q^4_{h_z}$ | 25.42 |
| $w_5$ | $Q_{l_z}Q^5_{h_z}$ | 13.46 |

[1] A. Suzuki and T. Tanaka, Nature (London) **346**, 345 (1990).

[2] S. Koshihara, Y. Tokura, T. Mitani, G. Saito, and T. Koda, Phys. Rev. B **42**, 6853(R) (1990).

[3] S. Decurtins, P. Gutlich, C. P. Kohler, H. Spiering, and A. Hauser, Chem. Phys. Lett. **105**, 1 (1984).

[4] K. Miyano, T. Tanaka, Y. Tomioka, and Y. Tokura, Phys. Rev. Lett. **78**, 4257 (1997).

[5] L. Stojchevska, I. Vaskivskyi, T. Mertelj, P. Kusar, D. Svetin, S. Brazovskii, and D. Mihailovic, Science **344**, 177 (2014).

[6] M. Rini, R. Tobey, N. Dean, J. Itatani, Y. Tomioka, Y. Tokura, R. W. Schoenlein, and A. Cavalleri, Nature (London) **449**, 72 (2007).

[7] A. D. Caviglia, R. Scherwitzl, P. Popovich, W. Hu, H. Bromberger, R. Singla, M. Mitrano, M. C. Hoffmann, S. Kaiser, P. Zubko *et al.*, Phys. Rev. Lett. **108**, 136801 (2012).

[8] R. I. Tobey, D. Prabhakaran, A. T. Boothroyd, and A. Cavalleri, Phys. Rev. Lett. **101**, 197404 (2008).

[9] M. Först, R. I. Tobey, S. Wall, H. Broberger, V. Khanna, A. L. Cavalieri, Y.-D. Chuang, W. S. Lee, R. Moore, W. F. Schlotter *et al.*, Phys. Rev. B **84**, 241104(R) (2011).

[10] M. Först, A. D. Caviglia, R. Scherwitzl, R. Mankowsky, P. Zubko, V. Khanna, H. Bromberger, S. B. Wilkins, Y.-D. Chuang, and W. S. Lee *et al.*, Nat. Mater. **14**, 883 (2015).

[11] D. Fausti, R. I. Tobey, N. Dean, S. Kaiser, A. Dienst, M. C. Hoffmann, S. Pyon, T. Takayama, H. Takagi, and A. Cavalleri, Science **331**, 189 (2011).

[12] S. Kaiser, C. R. Hunt, D. Nicoletti, W. Hu, I. Gierz, H. Y. Liu, M. Le Tacon, T. Loew, D. Haug, B. Keimer, and A. Cavalleri, Phys. Rev. B **89**, 184516 (2014).

[13] W. Hu, S. Kaiser, D. Nicoletti, C. R. Hunt, I. Gierz, M. C. Hoffmann, M. Le Tacon, T. Loew, B. Keimer, and A. Cavalleri, Nat. Mater. **13**, 705 (2014).

[14] M. Mitrano, A. Cantaluppi, D. Nicoletti, S. Kaiser, A. Perucchi, S. Lupi, P. Di Pietro, D. Pontiroli, M. Ricc, S. R. Clark, D. Jaksch, and A. Cavalleri, Nature (London) **530**, 461 (2016).

[15] J. T. Kindt and C. A. Schmuttenmaer, J. Chem. Phys. **110**, 8589 (1999).

[16] J. Orenstein and J. S. Dodge, Phys. Rev. B **92**, 134507 (2015).

[17] M. Först, C. Manzoni, S. Kaiser, Y. Tomioka, Y. Tokura, R. Merlin, and A. Cavalleri, Nat. Phys. **7**, 854 (2011).

[18] M. Först, R. Mankowsky, H. Bromberger, D. M. Fritz, H. Lemke, D. Zhu, M. Chollet, Y. Tomioka, Y. Tokura, R. Merlin, J. P. Hill, S. L. Johnson, and A. Cavalleri, Solid State Commun. **169**, 24 (2013).

[19] A. Subedi, A. Cavalleri, and A. Georges, Phys. Rev. B **89**, 220301(R) (2014).

[20] R. Mankowsky, A. Subedi, M. Först, S. O. Mariager, M. Chollet, H. T. Lemke, J. S. Robinson, J. M. Glownia, M. P. Minitti, A. Frano *et al.*, Nature (London) **516**, 71 (2014).

[21] R. F. Wallis and A. A. Maradudin, Phys. Rev. B **3**, 2063 (1971).

[22] T. P. Martin and L. Genzel, Phys. Status Solidi B **61**, 493 (1974).

[23] M. Fechner and N. A. Spaldin, Phys. Rev. B **94**, 134307 (2016).

[24] D. M. Juraschek, M. Fechner, and N. A. Spaldin, Phys. Rev. Lett. **118**, 054101 (2017).

[25] A. Subedi, Phys. Rev. B **92**, 214303 (2015).

[26] G. Kresse and J. Furthmüller, Phys. Rev. B **54**, 11169 (1996).

[27] P. E. Blöchl, Phys. Rev. B **50**, 17953 (1994).

[28] G. Kresse and D. Joubert, Phys. Rev. B **59**, 1758 (1999).

[29] J. P. Perdew, A. Ruzsinszky, G. I. Csonka, O. A. Vydrov, G. E. Scuseria, L. A. Constantin, X. Zhou, and K. Burke, Phys. Rev. Lett. **100**, 136406 (2008).

[30] K. Parlinski, Z.-Q. Li, and Y. Kawazoe, Phys. Rev. Lett. **78**, 4063 (1997).

[31] A. Togo, F. Oba, and I. Tanaka, Phys. Rev. B **78**, 134106 (2008).

[32] S. Baroni, S. de Gironcoli, A. Dal Corso, and P. Giannozzi, Rev. Mod. Phys. **73**, 515 (2001).

[33] X. Gonze and C. Lee, Phys. Rev. B **55**, 10355 (1997).

[34] J. W. Eaton, D. Bateman, S. Hauberg, and R. Wehbring, *GNU Octave Version 4.0.0 Manual: A High-Level Interactive Language for Numerical Computations* http://www.gnu.org/software/octave/doc/interpreter (2015).

[35] K. Takahashi, N. Kida, and M. Tonouchi, Phys. Rev. Lett. **96**, 117402 (2006).

[36] D. Talbayev, S. Lee, S.-W. Cheong, and A. J. Taylor, Appl. Phys. Lett. **93**, 212906 (2008).

[37] J. F. Scott, Rev. Mod. Phys. **46**, 83 (1974).

[38] E. Bousquet, M. Dawber, N. Stucki, C. Lichtensteiger, P. Hermet, S. Gariglio, J.-M. Triscone, and P. Ghosez, Nature (London) **452**, 732 (2008).

[39] D. J. Singh, Phys. Rev. B **53**, 176 (1996).

[40] H. Vogt and H. Uwe, Phys. Rev. B **29**, 1030 (1984).